International Journal for Research in Engineering Application & Management (IJREAM)
ISSN : 2454-9150 Vol-07, Issue-08, NOV 2021

# Deposition time effect on physical properties of Iron Disulfide ($FeS_2$) thin films grown by Chemical Bath Deposition

[1]C. Sumalatha, [2]G. Phaneendra Reddy, [3]K.T. Ramakrishna Reddy

[1,2]Research Scholar, [3]Professor, [1,2]Solar Energy Laboratory, Department of Physics, Sri Venkateswara University, Tirupati, Andhra Pradesh, India. [1]chava.sumalatha@gmail.com, [2]phaneendra369@gmail.com, [3]ktrkreddy@gmail.com

**Abstract** **Iron disulfide ($FeS_2$) films were deposited successfully on glass substrates at three different deposition times ($T_d$) that vary in the range, 2-4 h. In this work, we used iron chloride ($FeCl_3$), thioacetamide ($C_2H_5NS$) as precursors and tartaric acid with ammonia as a complexing agent. X-ray diffraction pattern revealed that the grown films were polycrystalline in nature by displaying many peaks, which are related to iron disulfide. The chemical stoichiometry of the deposited films was estimated using energy dispersive spectroscopy (EDS) analysis. The scanning electron microscopy studies revealed that the as-grown $FeS_2$ films were uniform and flower like densely packed grains over the surface. The optical investigations showed that the layers were highly absorbing with the optical absorption coefficient ~ $10^5$ $cm^{-1}$. A decrease in optical band gap from 1.66 eV to 1.54 eV with an increase of deposition time was observed. It is speculated that deposition time could play an important role in the film properties.**

***Keywords — $FeS_2$ thin films, Chemical bath deposition, XRD, SEM, FTIR, optical properties.***

## I. INTRODUCTION

In recent years, iron chalcogenides ($FeX_2$, X = S and Se) have generated lot of interest in research community across the world because of the involvement of many earth abundant elements. Further, these materials are more economical and ecological with adjustable magnetic, optical and electrical properties [1-4]. Basically iron showed seven main phases, while iron sulphides showed three dominant phases in terms of temperature, pressure, and high sulfur concentrations. Through the various crystalline phases of these compounds, the pyrite material $FeS_2$ with both cubic and orthorombic are promising materials for photovoltaic solar applications. $FeS_2$ solar cells can be made with an efficiency of 10%. $FeS_2$ has a higher absorption coefficient ($\alpha$) of $10^5$ $cm^{-1}$ than silicon, large minority carrier diffusion length of about 100-1000 nm and a suitable band gap ranging from 0.95 to 1.0 eV [4-13]. Therefore, $FeS_2$ is one of the best materials for large scale power generation at low cost. Since the rapid increase in energy demand results in the production of low cost solar cells based on less expensive, non-toxic and abundant elements, the use of $FeS_2$ and $FeSe_2$ can certainly meet these requirements.

Secondly, the nature and quality of pyrite films should strongly depend on the preparation methods [9]. Iron disulfide films were prepared by various researchers using reactive ion beam sputtering [14], electro deposition [15], sulfurization of iron thin films [16], sol-gel method [17] and chemical bath depostion [18-20]. Among these preparation methods, the chemical bath deposition is a low cost method and it is very easy to control the synthesis parameters during the growth of $FeS_2$ layers. In the current work, the deposition time ($T_d$) effect on physical properties of $FeS_2$ layers were studied for application of thin film solar cells.

## II. EXPERIMENTAL

$FeS_2$ thin films were prepared using chemical Bath deposition process and the various steps involved in it is shown in Fig.1. primarily, 20 ml of Analytical grade iron chloride ($FeCl_3$ with 0.6 M), 20 ml of thioacetamide ($C_2H_5NS$ with 0.6 M) and 10 ml of tartaric acid ($C_4H_6O_6$ with 1M) were prepared separately, the solution was taken into glass beaker using stirrer mechanism, after 5 min. 6 ml of ammonia hydroxide ($NH_4OH$) was added to the solution at conctant temperature of 85 $^oC$, varying the deposition time ($T_d$) in the rage, 2 - 4 h. The as grown $FeS_2$ films appeared the dark brownish green in color, soon after removing from the bath, which turn into orange yellow color within few minutes. The deposited $FeS_2$ layers were characterized using appropriate techniques to evaluate the physical behavior.

 DOI : 10.35291/2454-9150.2021.0590 

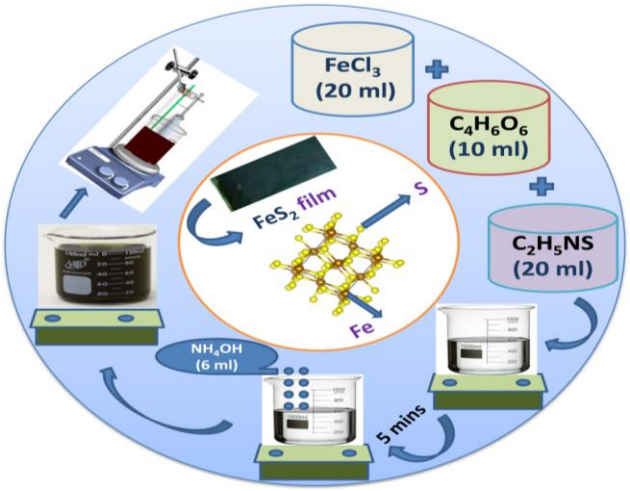


Figure 1. Experimental stages of the preparation of $FeS_2$ thin films.

## III. RESULTS AND DISCUSSION

*2.1. XRD analysis*

The X-ray diffraction pattern of $FeS_2$ films deposited on glass substrates, prepared at various deposition times ($T_d$) were recorded in the 2θ range of 10°-90° and is shown in Figure 2. It revealed that the grown films were polycrystalline in nature, showing multiple peaks corresponding to $FeS_2$ phases. The XRD patterns of films prepared at $T_d$ = 120 min showed peaks at 23.57° and 33.02° corresponding to (110) and (220) planes respectively. These peaks were closely matched with (#JCPDS card No. 03-0799) orthorhombic structure of $FeS_2$. With increase of the deposition time from 120 min. to 180 min., the peak position of 23.57° is shifted towards left. The observed peaks of 23.34° and 33.04° were corresponding to (111) and (200) planes of cubic $FeS_2$ (#JCPDS card no. 01-1295). The films prepared at $T_d$ = 240 min. showed peaks at 23.34°, 33.04° 40.78°, 47.33°, and 58.73° that correspond to (111), (200), (211), (220), and (222) planes respectively, and were related to the cubic $FeS_2$ structure.

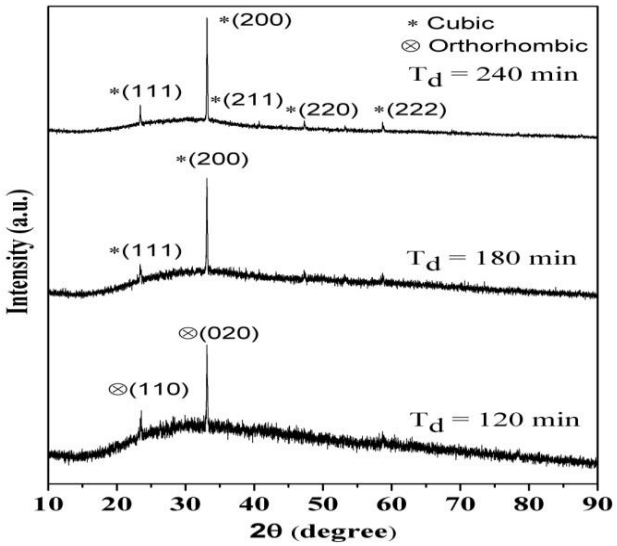


Figure 2. The XRD pattern of $FeS_2$ films.

Various structural parameters were calculated from the quantitative Rietveld refinement of XRD data using EXPO software.

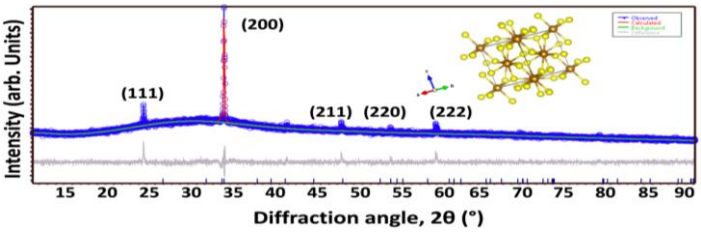


Figure 3. Rietveld refinement pattern of $FeS_2$ films prepared at $T_d$ = 240 min.

Some of the structural parameters were determined to confirm the cubic crystal structure to $FeS_2$ layers deposited at $T_d$ = 240 min and is shown in fig. 3. The goodness of fit (GOF) and R weighted profile ($R_{WP}$) values for fitting are 1.482 and, 6.597 % respectively. The site occupancies of various ions along with their fractional coordinates are given in table 1. A unit cell structure depicting the atomic coordination in the $FeS_2$ lattice in shown as an inset in figure 3. From the figure it can be noted that the layers crystallize in cubic crystal structure with P a-3 space group. Further, the atomic bonding parameters in cubic $FeS_2$ films were evaluated using Veesta software and are given in table 1. The study revealed that $FeS_2$ contain 70 atoms connected with 84 bonds and the related crystal structure is shown in figure 4.

Table 1: Structural parameters of $FeS_2$ obtained after Rietveld refinement

| Element | x | y | z | Occ. | Site | Sym. |
|---|---|---|---|---|---|---|
| Fe | 0.000 | 0.000 | 0.000 | 1.0 | 4a | -3. |
| S | 0.384 | 0.384 | 0.384 | 1.0 | 8c | -3. |

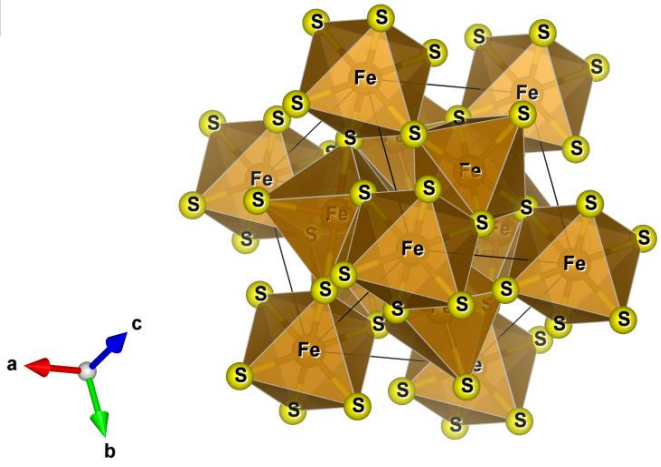


Figure 4. Distribution of Fe and S atoms in $FeS_2$ crystal.

The crystalline size (D) of the films was calculated using the Debye-Scherrer formula [21],

 DOI : 10.35291/2454-9150.2021.0590 

$$D = \frac{C\lambda}{\beta \cos\theta} \quad (1)$$

where $\beta$ is the full width at half maximum (FWHM) in radians, $\theta$ is diffraction angle, $\lambda$ is the wavelength of X-rays and C is the correction factor, which is taken as 0.9. The calculated crystallite size of $FeS_2$ films is given in table 2. The crystallite size was varied in the range of 55-84 nm with the increase of deposition time. Further, the dislocation density (δ), which is the number of dislocation lines per unit volume present in the deposited films was estimated using the relation [22],

$$\delta = \frac{1}{D^2} \quad (2)$$

The calculated values of dislocation density (δ) with deposition time, given in table 3 revealed that δ value decreased with increase of deposition time, which indicates that the good quality $FeS_2$ films with less defect density could be achieved at higher deposition times. The lattice mismatch occurred between the polycrystalline film and glass substrate is mostly due to the variation of lattice strain (ε), which is obtained by using the following relation,

$$\varepsilon = \frac{\beta \cos\theta}{4} \quad (3)$$

where θ is diffraction angle and $\beta$ is the full width at half maximum (FWHM) in radians. From the calculated results, it could be observed that the lattice strain decreases with the increase of the deposition time. The minimum value of ε was obtained for $T_d$ = 240 min, which indicates low lattice strain between the substrate and deposited $FeS_2$ films because of the change in nucleation mechanism and growth rate with increase of deposition time.

The stacking faults (SF), which are planar defects that characterize the disordering of crystallographic planes, were also determined for the experimental films by using the relation [23],

$$SF = \left[ \frac{2\pi^2}{45(3\tan\theta)^{\frac{1}{2}}} \right] \beta \quad (4)$$

where the symbols have their usual meening. The evaluated values of SF are listed in table 2, which shows that films prepared at a deposition time of 240 min. had low SF value than other films, this indicates that less planar defects were present in $FeS_2$ films prepared at this deposition time period.

Table 2. Variation of Crystallite size, Dislocation density, Lattice strain, and stacking faults as a function of deposition time.

| S. No. | $T_d$ (min.) | Crystallite size, D (nm) | Dislocation density, δ (lines/m$^2$) (x10$^{14}$) | Lattice strain (x10$^{-4}$) | stacking faults (x10$^{-4}$) |
|---|---|---|---|---|---|
| 1 | 120 | 55.47 | 3.24 | 3.26 | 6.32 |
| 2 | 180 | 67.62 | 2.18 | 2.68 | 5.18 |
| 3 | 240 | 84.53 | 1.39 | 2.14 | 4.14 |

### *2.2. Compositional analysis.*

The stoichiometry of the absorber material plays an important role in exhibiting the different crystal phases that in turn affect the performance of the developed solar cell device. Therefore, it is very important to know the elemental composition of the layer on order to optimize the deposition time to achieve the desired stoichiometry and crystallinity.

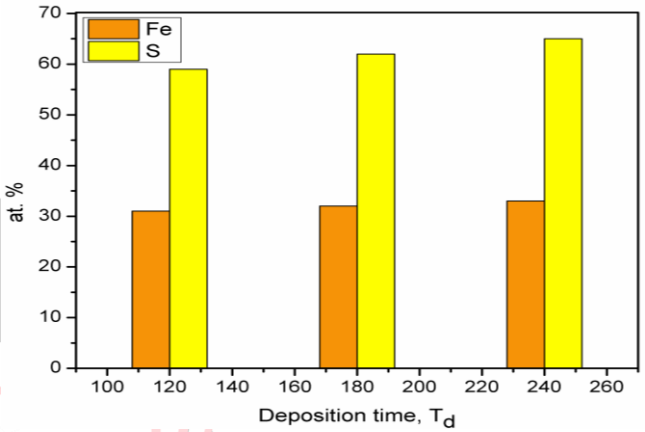


Figure 5. Elemental analysis of $FeS_2$ films prepared at different deposition times.

The EDS analysis indicated the presence of only Fe and S without any impurity elements at $T_d$ = 180 min and 240 min. although oxygen and silicon were found to be present at low deposition time (120 min). The determined composition of Fe and S in $FeS_2$ films using EDS spectra was shown in figure 5. Using bar diagrams, it can be observed from the figure that the composition of Fe and S was increased as a function of deposition time. The elemental composition in the films grown at $T_d$ = 240 min. was close to stoichiometric value.

### 2.3. Microstructure analysis.

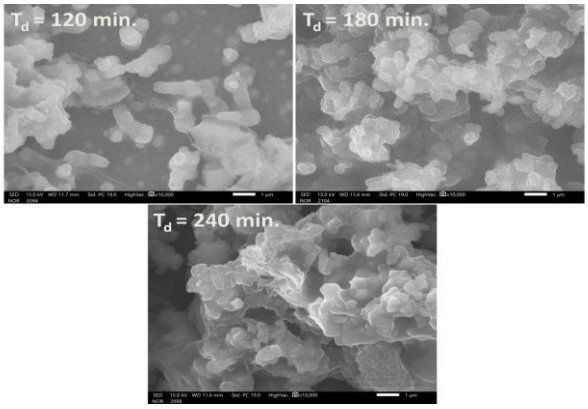


Figure 6. SEM images of $FeS_2$ films prepared at different deposition times.

 DOI : 10.35291/2454-9150.2021.0590 

The SEM micrographs of iron disulfide thin films formed at different deposition times are shown in Figure 6. The SEM images revealed that the films grown at $T_d$ = 120 min had irregular shaped grains. With increase of the deposition time, densely packed grains were observed. The surface of films prepared at $T_d$ of 240 min showed flower like grains. The grain sizes determined by SEM are in good agreement with the literature values and it proved to be the favorable morphology for efficient charge collection in solar cells.

### 2.4. FTIR analysis.

In order to monitor the phase conversion of the experimental samples, they were characterized by FTIR spectroscopy. The infrared spectroscopy provides clear evidence on the bonding electrons in the material. Figure 7 shows the Fourier Transform Infrared spectra of $FeS_2$ films grown at different deposition times. The FTIR spectrum exhibited a small peak around 3738 $cm^{-1}$ and 1080 $cm^{-1}$ due to -OH stretching mode. In addition to this band, another band at 2925 $cm^{-1}$ was also observed, which can be assigned to the C-H stretching modes [24]. In addition to this, a peak around 1750 $cm^{-1}$ was due to CH group and another band at 1370 $cm^{-1}$ due to symmetrical deformation of C-N group. The peak observed at 2326 $cm^{-1}$ is related to the iron disulfide.

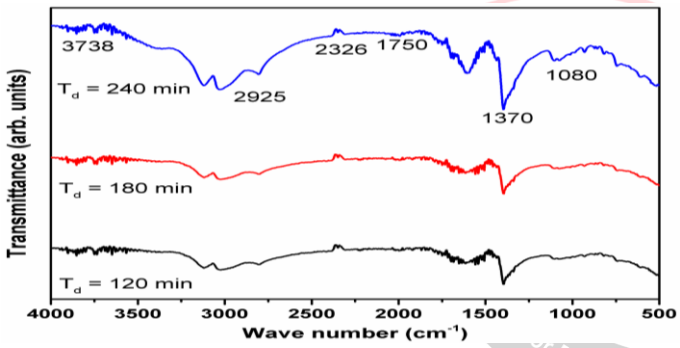


Figure 7. FTIR spectra of $FeS_2$ films prepared at different deposition times.

### 2.5. Optical Properties:

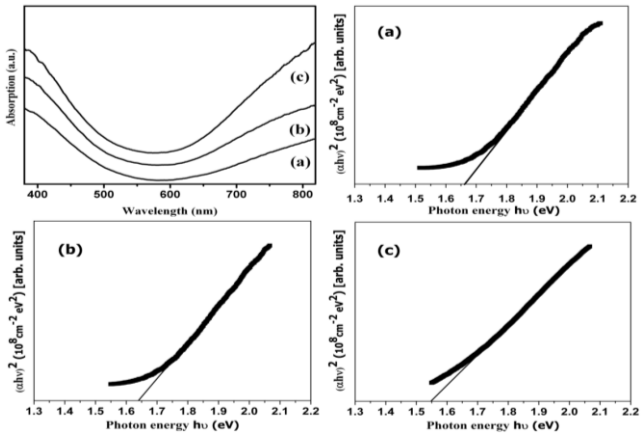


Figure 8. Absorption spectrum of $FeS_2$ films. And $(\alpha h\upsilon)^2$ versus hυ plots of $FeS_2$ films deposited at (a) $T_d$ = 120 min. (c) $T_d$ = 180 min and (d) $T_d$ = 240 min.

The optical absorption of the grown $FeS_2$ films formed on glass substrates at different deposition times was studied in the wavelength range, 350–850 nm is shown in fig. 8. From the figure it can be noted that the material exhibited sharp absorption edge in the visible wavelength region, indicating direct optical transition in this material. Further, the optical absorption of the films was higher than $10^4$ $cm^{-1}$ in visible region, which is highly needed for its use as an absorber in solar cells. The energy band gap of the films was evaluated using Tauc plots (shown in fig. 8 a,b & c) that decreased from 1.66 eV to 1.54 eV with the increase of $T_d$. The decrease of optical band gap with $T_d$ was attributed to the increase of crystallinity and packing density in the layers. The microstructural analysis discussed in the previous section confirmed this variation of packing density with deposition time in the experimental films.

## IV. Conclusions

$FeS_2$ thin films were successfully grown on glass substrates by chemical bath deposition method. The layers were formed at different deposition times that varied in the range, 180 – 240 min., keeping other growth parameters constant. XRD studies revealed the change of $FeS_2$ crystal structure from orthorhombic to cubic structure with increase of deposition time. SEM analysis exhibited an increase of grain size with deposition time, which supported the XRD analysis. FTIR spectra clearly indicated the presence of iron disulfide in the as-deposited layers along with other functional groups. The optical studies showed a direct optical absorption in the films, and the energy band gap decreased from 1.66 eV to 1.54 eV with the increase of bath temperature. The single phase $FeS_2$ films may find application as an absorber layer in the development of photovoltaic devices.

## References

[1] R. Azadar, A. Badshah, B. Lal, Fabrication, characterization and applications of iron selenide, *J. Solid State Chem.* 243 (2016) 179-189.

[2] W. Han, M. Gao, Investigations on iron sulfide nanosheetsprepared via a single-source precursor approach, *Cryst. Growth Des.*, 8 (2008) 1023-1030.

[3] C.E.M. Campos, J.C. De Lima, T.A. Grandi, K.D. Machado, P.S. Pizani, Structural studies of iron selenides prepared by mechanical alloying, *Solid State Communications*, 123 (2002) 179–184.

[4] B. Yuan, W. Luan, S.T. Tu, One-step synthesis of cubic $FeS_2$ and flower-like $FeSe_2$ particles by a solvothermal reduction process, *Dalt. Trans.*, 41 (2012) 772–776.

[5] H.J. Kwon, S. Thanikaikarasan, T. Mahalingam, K.H. Park, C. Sanjeeviraja, Y.D. Kim, Characterization of electrosynthesized iron diselenide thin films, *J. Mater. Sci. Mater.Electron.*, 19 (2008) 1086–1091.

[6] H.A. Macpherson, C.R. Stoldt, Iron pyrite nanocubes : size and shape considerations for photovoltaic application, *ACS Nano.* 6 (2012) 8940–8949.

 DOI : 10.35291/2454-9150.2021.0590 

[7] D. Jasion, J.M. Barforoush, Q. Qiao, Y. Zhu, S. Ren, K.C. Leonard, Low-dimensional hyperthin $FeS_2$nanostructures for efficient and stable hydrogen evolution electrocatalysis, *ACS Catal*., 5 (2015) 6653-6657.

[8] J. Choi, G. Cheruvally, H. Ahn, K. Kim, J. Ahn, Electrochemical characteristics of room temperature Li / FeS2 batteries with natural pyrite cathode, *J. Power Sources*., 163 (2006) 158–165.

[9] Z.P. Yin, K. Haule, G. Kotliar, Kinetic frustration and the nature of the magnetic and paramagnetic states in iron pnictides and iron chalcogenides, *Nat. Mater*., 10 (2011) 932-935.

[10] M.R. Gao, Y.F. Xu, J. Jiang, S.H. Yu, Nanostructured metal chalcogenides: synthesis, modification, and applications in energy conversion and storage devices, *Chem. Soc. Rev*., 42 (2013) 2986–3017.

[11] Y. Wang, J. Yang, H.K. Liu, W. Zhang, S.X. Dou, S. Chou, D. Zhao, Uniform yolk-shell iron sulfide–carbon nanospheres for superior sodium–iron sulfide batteries, *Nat. Commun*., 6 (2015) 8689.

[12] A. Photocatalyst, P. Fes, M. Barawi, I.J. Ferrer, E. Flores, S. Yoda, J.R. Ares, C. Sa, Hydrogen Photoassisted Generation by Visible Light and an Earth Abundant Photocalyst: Pyrite ($FeS_2$), *J. Phys. Chem. C*., 120 (2016) 9547-9552.

[13] E. Bastola, K.P. Bhandari, A.J. Matthews, N. Shrestha, R.J. Ellingson, Elemental anion thermal injection synthesis of nanocrystalline marcasite iron dichalcogenide $FeSe_2$ and $FeTe_2$, *RSC Adv*., 6 (2016) 69708-69714.

[14] Lichtenberger D, Ellmer K, Schieck R, Fiechter S, Tributsch H. *Thin Solid Films* 1994;246:6–12.

[15] Nakamura S, Yamamoto A. *Sol Energy Mat Sol C*ells 2001;65:79–85.

[16] Meng L, Liu YH, Tian L. *J Cryst Growth* 2003;253:530–8

[17] Huang, L., Wang, F., Luan, Z., & Meng, L. (2010). Pyrite (FeS2) thin films deposited by sol–gel method. *Materials Letters*, 64(23), 2612–2615. doi:10.1016/j.matlet.2010.08.07

[18] Aluri, V., Reddy, K. T. R., Reddy, Y. M. (2015) Polycrystalline and single phase FeS2 films grown by chemical bath deposition, *Nanotechnology Reviews*, 4(5), 469-472.

[19] Vedavathi, A., Ramakrishna Reddy, K. T., Munikrishna Reddy, Y. (2015) Role of ammonia on structural, electrical, FTIR and optical studies of FeS2 films formed by CBD, *International Organization of Scientific Research Journal of Engineering*, 05(02), 65-70.

[20] Kassim, A., Min, H. S., Yee, L. Y., Tee, T. W., Nagalingam, S. (2012) Complexing agent effect on the properties of iron sulphide thin films, *Canadian Journal of Pure and Applied Sciences*, 6(1), 1863-1867.

[21] H. Dahman, S. Rabaoui, A. Alyamani, L.E. Mir, Structural, morphological and optical properties of $Cu_2SnS_3$ thin film synthesized by spin coating technique, *Vacuum* 101 (2014) 208-211.

[22] G.B. Williamson, R.C. Smallman, III. Dislocation densities in some annealed and cold-worked metals from measurements on the X-ray debye-scherrer spectrum, *Phil. Mag.* 1 (1956) 34-46.

[23] M. Jothibas, C. Manoharan, S. Johnson Jeyakumar P. Praveen, I. Kartharinal, Punithavathy, J. Prince Richard, Synthesis and enhanced photocatalytic property of Ni doped ZnS nanoparticles, *Sol. Energy* 159 (2018) 434–443.

[24] Rath R K, Subramanian S and Pradeep T, 2000. *J. Colloid & Interface Sci*., 229 82-91.

 DOI : 10.35291/2454-9150.2021.0590 